An EXAFS Calculation Using Known Four-Body Correlations

P. W. Loeffen*,† and R. F. Pettifer

Department of Physics, University of Warwick, Coventry CV4 7AL, United Kingdom

(Received 19 September 1995)

An EXAFS calculation has been performed for the zinc tetraimidazole molecular cluster, which includes thermal four-body correlations, established from inelastic neutron scattering. Partial contributions to the fine structure are shown at several temperatures. Decompositions of the thermal damping in terms of the vibrational normal modes are given for individual scattering paths. Full vibrational information permits a quantitative comparison between theory and experiment without recourse to fitting. Differences between theory and experiment persist, setting limits on the systematic errors still present in theory.

PACS numbers: 61.10.Ht, 33.20.Rm, 78.70.Dm

Structural information is obtained from extended x-ray absorption fine structure (EXAFS) either by a comparison of an unknown compound with a known model (usually using Fourier transforms) or by fitting the spectrum directly to *ab initio* theory [1,2]. If multiple photoelectron scattering contributes to the EXAFS, then this implies the inclusion of three- or more-body correlation functions in the analysis, which can only realistically be accomplished using *ab initio* theory. Computer codes are available to generate the appropriate EXAFS signals theoretically [2–5] on which fitting algorithms can be built. However, in order to test their accuracy, it is important to input both the static *and* dynamic structural information *a priori*. Owing to the density of multiple scattering (MS) paths which may contribute to the final signal, fitting of thermal disorder parameters can produce artificial agreement with experiment. Explicit inclusion of thermal parameters thus provides a benchmark test of the accuracy of the theoretical models which underpin the *ab initio* approach to analysis. This is the first calculation of EXAFS to use an experimentally determined vibrational spectrum, which in this case comes from the reliable inelastic neutron scattering (INS) method.

The subject system in this work is the much studied zinc tetraimidazole complex. It was chosen due to its biological significance and its extensive MS which extends well into the EXAFS regime. Furthermore, its open structure and light atoms make it a particularly stringent test for the potential modeling. It typifies the type of system for which EXAFS is needed as a structural probe. The molecule consists of a central zinc atom with four five-membered imidazole rings coordinated in an approximately tetrahedral configuration. It is via INS from the four protons attached to each imidazole ring that we can sense and reliably determine the interatomic force field. INS has a very important advantage that the mean square displacement amplitudes of atomic motion are directly related to the spectral amplitude. Consequently, a vibrational force field may be established for the material such that both the eigenvectors and the eigenvalues are consistent with experiment. This is a far more sensitive test of the validity of the dynamical information [6] than simply equating the eigenvalues to the INS, infrared, or Raman peak positions. The product of such an analysis is the vibrational correlation function (VCF) which is a square matrix whose order is equal to the number of modes in the system, and it entirely describes all the many-body correlations within the harmonic approximation. INS has a further advantage since it clearly identifies those modes which are anharmonic and/or dispersive by spectral line broadening [6]. Exhaustive INS studies on this molecule have established the force field and are presented elsewhere [7,8].

EXAFS calculations without free parameters have been performed elsewhere using Debye and Einstein models [9,10], and cumulant expansions with and without spherical wave corrections and MS [11–15]. However, the full theory including MS and spherical wave propagators even in the harmonic approximation is complex. More recently, a MS treatment of general disorder effects has been given [16], including a many-body correlation which is based on a Taylor expansion of the amplitude and phase of scattering in terms of the generalized path coordinates. This approach provides a feasible and relatively simple computational scheme to link INS to EXAFS. We can explicitly calculate the temperature dependent fine structure from dynamic information provided by INS. In addition, we are able to determine the partial effect of thermal damping on individual scattering paths plus, for the first time, we obtain a clear description of the contributions to the damping of MS paths due to the many orthogonal modes of vibration. Our aim is to calculate the *ab initio* temperature-dependent total EXAFS spectra with no free parameters and to compare this to experiment. In this way, the quantum mechanical approximations involved in EXAFS can be measured.

Following Benfatto *et al.* [17], we write the nth partial contribution to the spherically averaged EXAFS fine structure $\chi_n(k)$ as

$$\chi_n(k) = A_n(k, \mathbf{r}) \sin\psi_n(k, \mathbf{r}) , \qquad (1)$$

where n runs over all paths including MS, $A_n(k, \mathbf{r})$ is an

 0031-9007/96/76(4)/636(4)$06.00

amplitude function, and $\psi_n(k, \mathbf{r})$ is a total phase function, both of which are in turn functions of generalized coordinates $\mathbf{r}$ and photoelectron wave number k. Using a first-order Taylor expansion of A_n and ψ_n, Benfatto, Natoli, and Filipponi [16] were able to obtain an analytical expression for the statistical average of χ_n over all configurations of the nth path based on a multivariate Gaussian distribution of the disorder, which in general can be both static and dynamic. In our specific case, we consider only thermal dynamic disorder within the harmonic approximation in which case the Gaussian distribution is exact. The configurationally averaged $\chi_n(k)$ is then written in normal coordinates, $\mathbf{Q}$, as

$$\langle \chi_n(k) \rangle = A_n(k, \mathbf{Q})|_{\mathbf{Q}=\mathbf{0}} [1 + F_1^2(k)]^{1/2} \times e^{-F_2(k)} \sin[\psi_n(k, \mathbf{Q})|_{\mathbf{Q}=\mathbf{0}} + F_1(k)], \quad (2)$$

where $F_1(k)$ and $F_2(k)$ involve the derivatives of A_n and ψ_n with respect to $\mathbf{Q}$ summed over the $3N - 6$ normal modes of N-atom molecular cluster and are given by

$$F_1(k) = \sum_{i=1}^{3N-6} \left[\frac{1}{A_n(k, \mathbf{Q})} \frac{\partial A_n(k, \mathbf{Q})}{\partial Q_i} \frac{\partial \psi_n(k, \mathbf{Q})}{\partial Q_i} \right]_{\mathbf{Q}=\mathbf{0}} [\mathbf{M}]_{ii} \quad (3)$$

and

$$F_2(k) = \frac{1}{2} \sum_{i=1}^{3N-6} \left(\frac{\partial \psi_n(k, \mathbf{Q})}{\partial Q_i} \bigg|_{\mathbf{Q}=\mathbf{0}} \right)^2 (\mathbf{M})_{ii}, \quad (4)$$

and $\mathbf{M}$ is the diagonalized vibrational correlation function whose elements are given by

$$[\mathbf{M}]_{ii} = \langle Q_{ii}^2 \rangle = \frac{\hbar}{2\omega_i} \coth\left(\frac{\hbar \omega_i}{2k_B T} \right), \quad (5)$$

where ω_i is the vibrational eigenvalue which corresponds to the eigenvector Q_i, and T is the temperature. All that remains is to evaluate the coefficients A_n, ψ_n, F_1, and F_2 for two static configurations, and these come from *ab initio* MS calculations. The derivatives in F_1 and F_2 are established numerically for each normal mode by calculating A_n and ψ_n at the equilibrium (denoted $\mathbf{Q} = \mathbf{0}$) and at a root mean square displacement in $\mathbf{Q}$-configuration space. The first-order truncation of the Taylor expansion, used to derive Eq. (2), was justified by explicit calculations for the temperatures and force field used here.

All codes currently available [2–5] solve the scattering problem of a suitably dressed electron moving in and between muffin-tin (MT) potentials. In this particular case, we chose the MSXAS package [4], in which the one electron MT potential is constructed by solving Poisson's equation for the spherically symmetrized overlapped free atom electron densities in the crystallographic configuration of zinc tetraimidazole. The MT radii were chosen using the Norman criterion times a factor of 0.8. These parameters were the default for the code, and resulted in no overlap in the MT radii between the zinc and nitrogen atoms, but a 0.25 to 0.3 Å overlap of MT spheres for atoms within the imidazole ring. The final state potential sensed by the photoelectron was constructed using the $Z + 1$ approximation with the exchange-correlation (XC) potential from Hedin and Lundqvist [18,19]. Within the MT approximation, the scattering was calculated using 20 partial wave phase shifts and retains all curved wave effects. No $|S_0|^2$ term was included to model the multielectron excitations in the photoabsorbing atom, but the imaginary part of the emitter phase shift was included. Core hole lifetime effects were modeled assuming a value of 0.95 eV.

Figure 1 is a schematic of one imidazole branch including the central zinc. Two inequivalent imidazole branches were considered in the dynamical analysis due to the twofold crystallographic symmetry. All of the possible 160 intrabranch paths up to order 3 were calculated, and the 60 most important were retained based on the peak amplitudes of the k^3-weighted partial contributions in the range $k = 4$–18 Å^{-1}. Interbranch scattering was neglected apart from the strong Zn-N-N-Zn double scattering path, where the nitrogen atoms (N) are directly bonded to zinc. We also found that many paths not included in this calculation made a contribution in the low k part of the spectrum. The difference between our path subset and a complete calculation including all scattering up to fifth order was less than 3.5% in the total EXAFS.

Figure 2 shows the calculated k^3-weighted partial contributions to the total EXAFS from the seven most important paths in one imidazole branch. The solid lines show the configurationally averaged signals, $\langle \chi_n(k) \rangle$, at seven temperatures between 20 and 300 K compared with the static scattering signal, $\chi_n(k)$. It is clear from Fig. 2 that MS terms survive out to $k = 18$ Å^{-1} when the full vibrational analysis is performed and confirms earlier calculations [20,21] which did not benefit from the appropriate dynamic information. It can also be seen that the damping is most pronounced at high k. An examination of the F_1 and F_2 terms of Eq. (2) shows that the largest values of F_1 generally occur at low k, and they normally do not contribute more than 0.04% to the amplitude of the signal, although some exceptions for small amplitude paths have been observed, e.g., path 1 4 5 1. Consequently, the damping is dominated by F_2 and the exponential term which contains it has the form of the normal Debye-Waller type term.

In Fig. 3, the breakdown of the contributions to the F_2 functions from the 105 vibrational normal modes is shown for the same seven paths as in Fig. 2. The 105 components

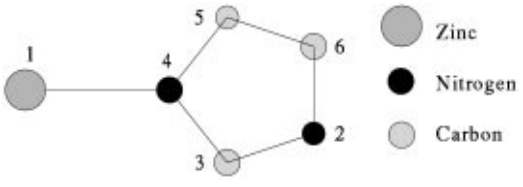

FIG. 1. One imidazole branch defining the atomic labeling.

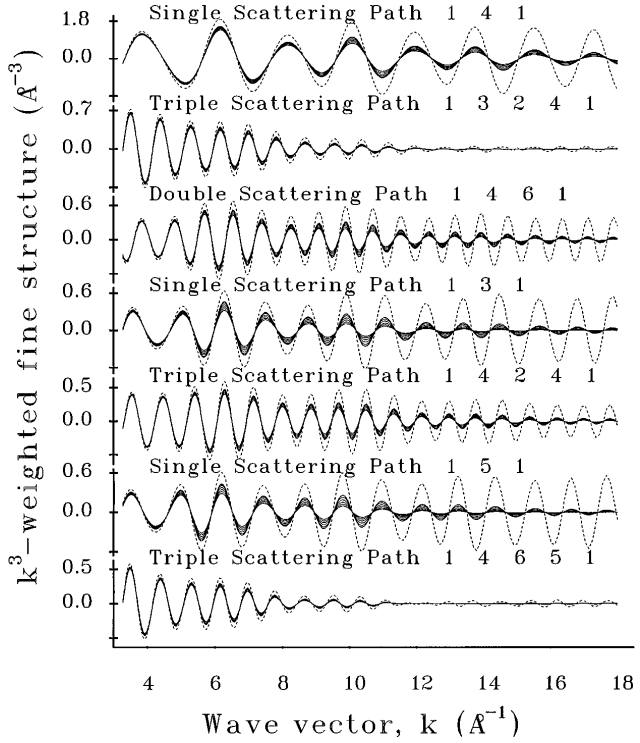

FIG. 2. k^3-weighted partial contributions to the total EXAFS due to the seven most important scattering paths in one of the imidazole branches. Calculated signal with no treatment of thermal disorder (dashed line) compared to the configurationally averaged signals at seven temperatures between 20 and 300 K.

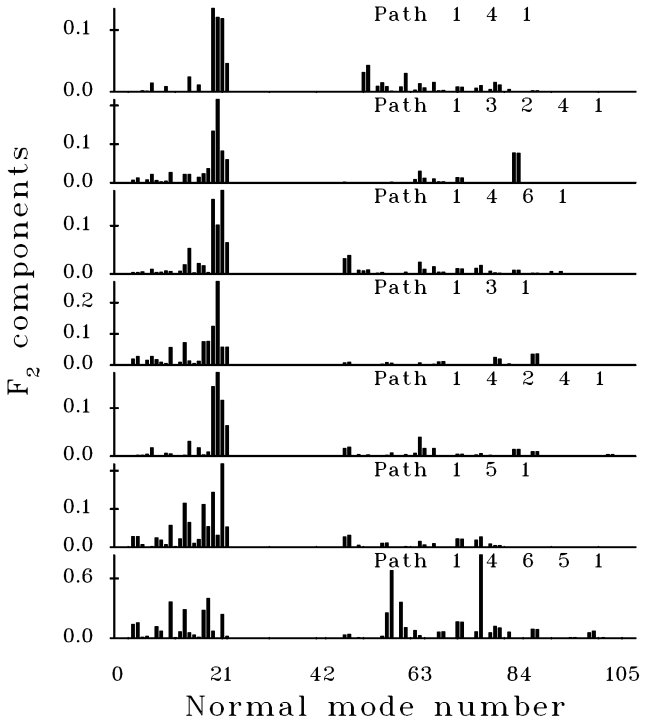

FIG. 3. Normal mode contributions to F_2.

of each of the bar charts are ordered from left to right in increasing frequency and were evaluated at $k = 12$ Å^{-1} and 20 K. It is evident from Fig. 3 that for most paths the dominant source of the damping is due to the cluster of four modes, numbered 18–21, which correspond to the Zn-N tetrahedral stretch modes of the molecule and occur in the range $225 - 300$ cm^{-1}. The lowest frequency modes, numbered 1–12, correspond to whole imidazole librations below 160 cm^{-1} and may be anharmonic and/or dispersive, but, as may be seen from Fig. 3, they do not contribute more than (5–10)% to the total of F_2 for the path except in a few cases, such as paths 1 5 1 and 1 4 6 5 1 where the contribution is about 20%. The modes above 160 cm^{-1} are believed to be harmonic and nondispersive due to the absence of line broadening in the INS spectrum. Modes 22–105 correspond to the internal imidazole ring vibrations (>600 cm^{-1}) of which only the in-plane modes, numbered 46–105 (>900 cm^{-1}), contribute. Thus, the damping due to the internal imidazole modes is small but not insignificant (e.g., for the Zn-N backscattering path 1 4 1 at 20 K, 35% of the F_2 term is due to internal ring modes). A notable anomaly is the path 1 4 6 5 1 (see Fig. 3), where the damping due to internal imidazole vibrations at 20 K exceeds that due to low frequency skeletal modes.

Experimental data were measured at the magic angle [22] on the EXAFS beamline of EMBL for seven temperatures. The measured energy resolution of the spectrometer was 1.7 eV, and the data were absolutely energy calibrated [23] to ± 0.2 eV over the entire spectrum. The superposed partial signals for the entire molecule were added to generate the total EXAFS at seven different temperatures which are plotted together with the experimental data in Fig. 4. Although there appears to be coarse agreement between theory and experiment, there are also trends of disagreements. In particular, it is clear that the amplitude of the calculated signal at high k is less than the measured signal. This can be traced to at least two sources of error. The first is the overestimate of the imaginary scattering component by the Hedin-Lundqvist XC potential. Second, a closer inspection of the amplitude of scattering showed that many of the potentials exhibited an amplitude fluctuation caused by the MT discontinuity. The modulation was of the order of $\pm 25\%$ of the k^3-weighted amplitude and extends to high k. Thus, it is clear that for open clusters containing low Z scatterers, the perturbation caused by the MT approximation is a problem in both the EXAFS as well as the XANES region. However, these two points are not sufficient to explain the lack of general agreement. In particular, features appear overemphasized in the low k region. This is in agreement with a previous study in this energy regime, despite a completely different code being used to generate the scattering phase shifts and partial fine structures [20]. Also, it should be noted that in the previous study potential discontinuities at the MT boundaries had been removed and inelastic loss was modeled with a constant imaginary self-energy of the photoelectron.

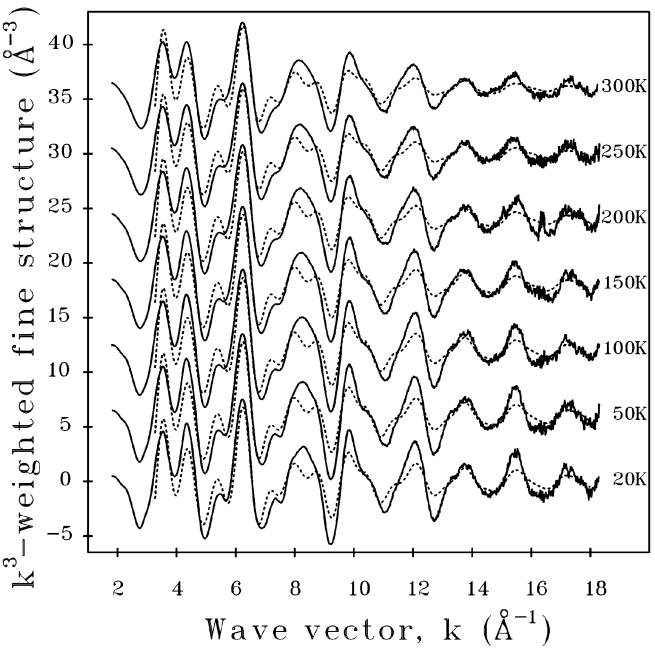

FIG. 4. Experimental and calculated (dashed) EXAFS of the zinc tetraimidazole tetrafluoroborate compound.

We conclude that the quality of the effective one electron potentials used in this study of light atom scattering EXAFS are inadequate for meaningful structural determination for atoms lying beyond the first shell as these contribute scattering signals comparable to the size of the discrepancies between theory and experiment which have been observed. As such this study points to the need to develop *potentials* free from muffin-tin effects possibly incorporating self-consistency in the electron density which are transferable between similar materials [24]. We also conclude that extensive fitting of path variances, which is currently employed, is not justified by the quality of the physical approximations.

*Also at EMBL c/o DESY, Notkestraße 85, 22603 Hamburg, Germany.

†Present address: ESRF, B.P. 220, F-38043 Grenoble Cédex, France.

[1] A. Filipponi, A. Di Cicco, T. A. Tyson, and C. R. Natoli, Solid State Commun. **78**, 265 (1991).

[2] S. J. Gurman, N. Binsted, and I. Ross, J. Phys. C **17**, 143 (1984).

[3] J. Mustre de Leon, J. J. Rehr, S. I. Zabinsky, and R. C. Albers, Phys. Rev. B **44**, 4146 (1991).

[4] M. F. Ruiz-López, F. Bohr, A. Filipponi, A. Di Cicco, T. A. Tyson, M. Benfatto, and C. R. Natoli, in *X-ray Absorption Fine Structure*, edited by S. S. Hasnain (Ellis-Horwood, New York, 1991).

[5] R. V. Vedrinskii, L. A. Bugaev, and I. G. Levin, Phys. Status Solidi B **150**, 307 (1988).

[6] P. A. Reynolds, J. K. Kjems, and J. W. White, J. Chem. Phys. **56**, 2928 (1972).

[7] P. W. Loeffen, R. F. Pettifer, F. Fillaux, and G. J. Kearley, J. Chem. Phys. **103**, 8444 (1995).

[8] P. W. Loeffen, R. F. Pettifer, and J. Tomkinson (to be published).

[9] G. Beni and P. M. Platzman, Phys. Rev. B **14**, 1514 (1976).

[10] E. Sevillano, H. Meuth, and J. J. Rehr, Phys. Rev. B **20**, 4908 (1979).

[11] P. Eisenberger and G. S. Brown, Solid State Commun. **29**, 481 (1979).

[12] V. Fritzsche, J. Phys. Condens. Matter **2**, 9735 (1990).

[13] P. Rennert, J. Phys. Condens. Matter **4**, 4315 (1992).

[14] C. Brouder, J. Phys. C **21**, 5075 (1988).

[15] T. Fujikawa, M. Yimagawa, and T. Miyanaga, J. Phys. Soc. Jpn. **64**, 2047 (1995).

[16] M. Benfatto, C. R. Natoli, and A. Filipponi, Phys. Rev. B **40**, 9626 (1989).

[17] M. Benfatto, C. R. Natoli, A. Bianconi, J. Garcia, A. Marcelli, M. Fanfoni, and I. Davoli, Phys. Rev. B **34**, 5774 (1986).

[18] L. Hedin and S. Lundqvist, Solid State Phys. **23**, 1 (1969).

[19] S. H. Chou, J. J. Rehr, E. A. Stern, and E. R. Davidson, Phys. Rev. B **35**, 2604 (1987).

[20] R. F. Pettifer, D. L. Foulis, and C. Hermes, J. Phys. (Paris) **47**, 545 (1986).

[21] R. W. Strange, N. J. Blackburn, P. F. Knowles, and S. S. Hasnain, J. Am. Chem. Soc. **109**, 7157 (1987).

[22] R. F. Pettifer, C. Brouder, M. Benfatto, C. R. Natoli, C. Hermes, and M. F. Ruiz-López, Phys. Rev. B **42**, 37 (1990).

[23] R. F. Pettifer and C. Hermes, J. Appl. Crystallogr. **18**, 404 (1985).

[24] D. L. Foulis, R. F. Pettifer, and P. Sherwood, Europhys. Lett. **29**, 647 (1995).